

Article

# 3D Printed Thermoelectric Polyurethane/Multiwalled Carbon Nanotube Nanocomposites: A Novel Approach towards the Fabrication of Flexible and Stretchable Organic Thermoelectrics

Lazaros Tzounis <sup>1,\*</sup>, Markos Petousis <sup>2</sup> , Sotirios Grammatikos <sup>3</sup>  and Nectarios Vidakis <sup>2,\*</sup>

<sup>1</sup> Composite and Smart Materials Laboratory (CSML), Department of Materials Science & Engineering, University of Ioannina, GR-45110 Ioannina, Greece

<sup>2</sup> Mechanical Engineering Department, Hellenic Mediterranean University, Estavromenos, 71004 Heraklion, Crete, Greece; markospetousis@hmu.gr

<sup>3</sup> Group of Sustainable Composites, Department of Manufacturing and Civil Engineering, Norwegian University of Science and Technology, 2815 Gjøvik, Norway; sotirios.grammatikos@ntnu.no

\* Correspondence: latzounis@uoi.gr (L.T.); vidakis@hmu.gr (N.V.);  
Tel.: +30-26-5100-9024 (L.T.); +30-2810-379-833 (N.V.)

Received: 4 June 2020; Accepted: 24 June 2020; Published: 26 June 2020



**Abstract:** Three-dimensional (3D) printing of thermoelectric polymer nanocomposites is reported for the first time employing flexible, stretchable and electrically conductive 3D printable thermoplastic polyurethane (TPU)/multiwalled carbon nanotube (MWCNT) filaments. TPU/MWCNT conductive polymer composites (CPC) have been initially developed employing melt-mixing and extrusion processes. TPU pellets and two different types of MWCNTs, namely the NC-7000 MWCNTs (NC-MWCNT) and Long MWCNTs (L-MWCNT) were used to manufacture TPU/MWCNT nanocomposite filaments with 1.0, 2.5 and 5.0 wt.%. 3D printed thermoelectric TPU/MWCNT nanocomposites were fabricated through a fused deposition modelling (FDM) process. Raman and scanning electron microscopy (SEM) revealed the graphitic nature and morphological characteristics of CNTs. SEM and transmission electron microscopy (TEM) exhibited an excellent CNT nanodispersion in the TPU matrix. Tensile tests showed no significant deterioration of the moduli and strengths for the 3D printed samples compared to the nanocomposites prepared by compression moulding, indicating an excellent interlayer adhesion and mechanical performance of the 3D printed nanocomposites. Electrical and thermoelectric investigations showed that L-MWCNT exhibits  $19.8 \pm 0.2 \mu\text{V/K}$  Seebeck coefficient ( $S$ ) and  $8.4 \times 10^3 \text{ S/m}$  electrical conductivity ( $\sigma$ ), while TPU/L-MWCNT CPCs at 5.0 wt.% exhibited the highest thermoelectric performance ( $\sigma = 133.1 \text{ S/m}$ ,  $S = 19.8 \pm 0.2 \mu\text{V/K}$  and  $PF = 0.04 \mu\text{W/mK}^2$ ) among TPU/CNT CPCs in the literature. All 3D printed samples exhibited an anisotropic electrical conductivity and the same Seebeck coefficient in the through- and cross-layer printing directions. TPU/MWCNT could act as excellent organic thermoelectric material towards 3D printed thermoelectric generators (TEGs) for potential large-scale energy harvesting applications.

**Keywords:** conductive polymer composites (CPCs); three-dimensional (3D) printing; 3D printed thermoelectrics; polymer thermoelectrics; flexible and stretchable thermoelectrics

## 1. Introduction

Three-dimensional (3D) printing has dramatically expanded over the last 20 years, while currently being a cutting-edge and one of the most widely used additive manufacturing (AM) technologies amongst others [1]. 3D printed parts and components due to variable mechanical and physicochemical

properties that can be achieved could be employed in a wide range of applications [2]. A significant technological progress has been made for fused deposition modelling (FDM) printers and related machinery; however, a rapid growth has occurred lately towards the development of functional and novel printable thermoplastic materials, i.e., electrically conductive [3], magnetically active [4], flexible and stretchable [5], etc., filaments. Conductive polymer composites (CPCs) are known to offer various sensing functionalities, i.e., touch and pressure, temperature, chemical and/or electrochemical sensors [6]. Recently, electrically conductive filaments have been fabricated by employing carbon nanotubes (CNTs) and graphene as conductive filler incorporated in polylactide thermoplastic polymer matrix [7]. Moreover, CPC filaments have been reported for applications such as fabrication of FDM 3D printed strain sensors [8], resistors [9], biomedical sensors [10] and actuators [11].

Thermoelectric materials are by definition transducers of thermal to electrical energy being, thus capable of harvesting thermal energy and converting it into usable electricity. Specifically, thermoelectrics have the ability to generate an electric potential (known as thermoelectric voltage) upon being exposed to a temperature gradient, otherwise defined as the “Seebeck effect” [12]. It could be realised then that a high electrical conductivity ( $\sigma$ ) combined with high Seebeck coefficient ( $S = \Delta V/\Delta T$ ) and low thermal conductivity ( $\kappa$ ) are required for an efficient thermoelectric material. Traditional thermoelectric materials are typically based on low energy band gap inorganic semiconductors, e.g., Bi<sub>2</sub>Te<sub>3</sub> [13], PbTe [14], GeTe [15], etc.; however, such materials do not allow potential applications for energy harvesting on a large-scale, since they consist of rare and high toxicity elements. The introduction of organic materials and especially CNTs as fillers in thermoplastic polymer matrices endowed CPCs with thermoelectric property and this is a field of research that has emerged over the last decade [16,17]. Namely, SWCNTs incorporated via solvent mixing in a non-conductive polycarbonate (PC) polymer matrix exhibited an electrical conductivity of approx. 1000 S/m and Seebeck coefficient  $S = +60 \mu\text{V/K}$  at 30 wt.% SWCNT loading [18].

CPCs based on polymeric matrices having electron-donating functional groups, as for instance Polyvinyl alcohol (PVA) and polyethyleneimine (PEI), showed n-type thermoelectric behaviour. Specifically, PEI/SWCNT nanocomposites with PEI functioning as n-doping to the incorporated SWCNTs resulted in Seebeck coefficients up to  $-21.5 \mu\text{V/K}$  [19]. Previous research from our group investigating the thermoelectric properties of melt-mixed polycarbonate (PC)/MWCNT CPCs at different MWCNT loadings, showed that higher CNT contents resulted in increased power factors ( $PF = \sigma \times S^2$  in  $\text{W/mK}^2$ ), which has been mainly explained by the increase of the electrical conductivity [20]. In another study, high-performance polyetherimide–SWCNT thermoplastic CPCs have been reported capable of operation up to 200 °C with electrical conductivity reaching 20 S/m and Seebeck coefficients  $+55 \mu\text{V/K}$  at 10 wt.% SWCNT loading [21]. Moreover, flexible thermoelectric devices based on serially interconnected p- and n-doped SWCNT thermocouples have been reported [22], as well as flexible semiconductor fibres for temperature sensing [23]. Recently, a detailed review article has elaborated the novelty of thermoelectric composites based on conducting polymer/carbon nanoparticle systems as promising green energy materials [24]. CPC filaments for FDM 3D printing and 3D objects have been reported so far [25]; however, 3D printed thermoelectric polymer nanocomposites that can be flexible and stretchable at the same time have not been reported yet.

In this study, TPU/MWCNT 3D printable, flexible, stretchable and thermoelectric filaments have been developed with two different types of commercially available MWCNTs, while 3D printed thermoelements were fabricated and fully characterised. Two different MWCNTs were utilised (NC-MWCNT and L-MWCNT) with significant differences in electrical conductivity, while both were introduced in a TPU matrix via a melt compounding/mixing process. Masterbatches of 5.0 wt.% TPU/NC-MWCNT and TPU/L-MWCNT were produced initially and in a next step reprocessed and diluted via melt mixing towards being finally extruded as filaments for the 3D printing process. SEM and transmission electron microscopy (TEM) exhibited the excellent nanocomposite microstructures (TPU/NC-MWCNT and TPU/L-MWCNT) with highly dispersed CNTs in the TPU matrix and without agglomerates that can affect the 3D printing process. All 3D printed samples

exhibited an anisotropic electrical conductivity and same Seebeck coefficient since it is an inherent material property arising from the CNT filler. The 3D printed TPU/MWCNT thermoelements printed herein can be the building blocks for the fabrication of flexible and stretchable organic thermoelectric generators (TEGs).

## 2. Materials and Methods

### 2.1. Materials

TPU pellets and MWCNTs of two different types with different graphitization degrees and lengths were used as the constituents of the conductive polymer nanocomposites (CPNs) fabricated in this study. Namely, Elastollan 1185A grade of TPU polymer having a density of  $1.12 \text{ g/cm}^3$  and a shore hardness of 85A was received by BASF and utilised as the matrix of the nanocomposites. Commercially available MWCNTs, namely NC7000 and long MWCNTs—hereafter denoted as NC-MWCNTs and L-MWCNTs, respectively—were purchased from Nanocyl S.A. (Sambreville, Belgium). According to the supplier specifications, both MWCNT grades exhibited purity higher than 90%. The NC-MWCNTs is a highly conductive grade material with CNTs exhibiting average diameters of 9.5 nm and average lengths of  $1.5 \mu\text{m}$ . NC-MWCNTs have been widely used elsewhere for melt-mixed conductive polymer composites (CPCs) [26–28]. The L-MWCNTs according to the supplier have slightly higher graphitization degree with CNTs of 9.5 nm in average diameter and consisting of longer CNTs with average lengths of  $3.0 \mu\text{m}$ .

### 2.2. Fabrication of TPU/NC-MWCNT and TPU/L-MWCNT Filaments

TPU/5 wt.% MWCNT masterbatches (NC-MWCNT and L-MWCNT respectively) were produced initially using a small-scale twin-screw extruder (ZSC 20, Noris Plastic GmbH, Nürnberg, Germany). The melt temperature was 219–228 °C and screw rotational speed 300 rpm, while a screw length-to-diameter (L/D) ratio of 36 was employed for the melt mixing process. The TPU/CNT masterbatch preparation process parameters were followed as reported elsewhere [8]. All materials used for the masterbatch production were premixed in a glass vial and placed in a vacuum oven at 80 °C overnight, prior to the compounding process. TPU/MWCNT nanocomposites with MWCNT content of 1.0, 2.5 and 5.0 wt.% with diluted concentrations from the masterbatch were prepared then using a DSM Xplore Microcompounder (Geleen, Netherlands). The microcompounder used had a capacity of  $15 \text{ cm}^3$  with conical twin screws of 150 mm length and L/D ratio of 18. The following parameters were applied for the mixing/masterbatch dilution process: 230 °C as the mixing temperatures, of 5 min in total as the mixing time at a constant rotational speed of the screws set at 150 rpm. The extruded filaments were finally wound up utilising a Filabot spooler (Filabot, Vermont), while the extrusion parameters were also optimized in order to achieve a constant filament diameter at various MWCNT contents. This is a prerequisite for FDM printers that require consistent filament diameter for the calculation of the feed rate during the printing process. The extruded filament diameter was measured to be in all cases  $1.68 \pm 0.07 \text{ mm}$ , which is adequate accuracy for consistent printing. This diameter was inserted in the slicer program to calculate the necessary feed rate that should be automatically used during the whole printing process. Neat TPU filament was prepared in the same manner.

### 2.3. Fused Deposition Modeling (FDM) of TPU/MWCNT Nanocomposites

A MakerBot Replicator 2 Experimental FDM printer (MakerBot, Brooklyn, NY, USA) and the MakerBot MakerWare software capable of processing STL files into thin slices to generate the G-code were used for 3D printing the TPU/MWCNT nanocomposite filaments. For optimum printability, the FDM printing parameters had to be initially optimized and finally the following printing conditions have been employed for all the printing processes in this study: nozzle temperature, 220 °C; print nozzle diameter, 0.8 mm; bed temperature, 60 °C; layer height, 0.20 mm; print infill, 100%; and print speed, 20 mm/s. The dimensions of the samples for the electrical conductivity and Seebeck coefficient measurements were  $1.6 \times 1.6 \text{ mm}$  with a length of 100 mm. All 3D models for the 3D printing in this

work have been designed using the 3D design Autodesk® Fusion 360™ (Autodesk®, Inc., San Rafael, CA, USA) software, while being finally exported to Standard Tessellation Language (STL) files.

#### 2.4. Characterization Techniques

A DXR Smart Raman instrument (Thermo Scientific, Waltham, MA, USA) was used to investigate the Raman spectroscopic responses of NC-MWCNT and L-MWCNT in this study. The spectra were acquired using a 532-nm laser line in the spectral region of 900–3000  $\text{cm}^{-1}$  with a laser spot diameter of  $\sim 3 \mu\text{m}$ , while the spectral resolution achieved was  $5 \text{ cm}^{-1}$ .

A JEOL JSM 6510 LV SEM/Oxford Instruments scanning electron microscope (SEM) (Jeol, Tokyo, Japan) operating at an accelerating voltage of 1.0 KV was employed for all the SEM investigations performed in this study. SEM was employed to study the morphology of NC-MWCNTs and L-MWCNTs in the form of bucky paper films, as well as for the TPU/MWCNT microstructural analysis to illustrate the nanotube dispersion in the TPU matrix. Cryo-fractured surfaces were prepared by immersing the samples in liquid nitrogen and broken perpendicular to the Y-printing direction. Transmission electron microscopy (TEM) (Libra 200 HR-TEM, Carl Zeiss AG, Oberkochen, Germany) analysis was performed in order to evaluate the MWCNT nanodispersion state in the TPU polymer matrix. Ultrathin sections of the polymer nanocomposites with a thickness of  $\sim 70 \text{ nm}$  were prepared by means of cryo-ultramicrotomy using an ultramicrotome (Leica UC7, Leica Microsystems GmbH, Wetzlar, Germany), while more details could be found elsewhere [29,30]. The thin sections were placed on copper grids (300 mesh Cu, Agar), and further investigated with an FEI microscope operating at an acceleration voltage of 100 kV.

The electrical conductivity of NC-MWCNTs and L-MWCNTs in the form of rectangular-shaped films (30.0 mm length  $\times$  5.0 mm width with thickness:  $\sim 100 \mu\text{m}$ ) was determined by measuring the room temperature sheet resistance ( $R_s$ ) using a four-point probe system (Ossila Ltd., Sheffield, UK). NC-MWCNT and L-MWCNT bucky paper films were prepared initially employing a vacuum filtration apparatus using polycarbonate filter membranes (0.4  $\mu\text{m}$  pore size) and 500 mL of CNT dispersions (0.3 mg/mL) with the help of SDBS surfactant (50% in relation to the CNT mass) and 30 min of bath sonication (Figure 1a). The filter cakes were cleaned with 20 mL of 30% hydrochloric acid (HCl) in order to remove the surfactant molecules, while 5 L of distilled water were filtered through the CNT films until reaching a neutral pH. The bucky papers were dried in a vacuum oven at 80 °C overnight and rectangular-shaped NC-MWCNT and L-MWCNT samples were cut for the sheet resistance derived electrical conductivity ( $\sigma$ ) measurements (bucky paper film thickness  $\sim 100 \mu\text{m}$ ). For the thermovoltage and electrical conductivity investigations of the TPU/MWCNT nanocomposites, the extruded filaments were cut into small pieces and thermally pressed under vacuum into circular-shaped samples with the following dimensions: 25.0 mm in diameter and 3.0 mm thickness. For all samples, the compression moulding temperature was 220 °C for 10 s and the pressure was set at 17.5 kN. The disks' flat surfaces were coated then with low-temperature and fast curing silver paste (Agar scientific, Germany) to contact the samples, while the samples with specific dimensions resistance was measured using an Agilent Multimeter (Agilent 34401A6 $\frac{1}{2}$ , Agilent, Santa Clara, CA, USA) in order to derive further the electrical resistivity ( $\rho$ ) and conductivity ( $\sigma$ ). The through-thickness (through-layer) as well as in-plane (cross-layer) electrical conductivity of 3D printed samples was determined using square-shaped samples of 15.0  $\times$  15.0  $\text{mm}^2$  and 3.0 mm thickness. In both cases, the appropriate surfaces were coated with Ag paste, as illustrated in Figure 1b, and the conductivity was derived from a two-point probe electrical resistance measurements. This was performed in order to elucidate if there is any loss in "bulk" electrical conductivity resulting further into an anisotropic electrical conductivity behaviour due to the FDM printing process.

A self-made custom set-up was employed to determine the Seebeck coefficient for all conductive samples in this work. NC-MWCNT and L-MWCNT bucky paper films (30.0 mm length  $\times$  5.0 mm width with thickness:  $\sim 100 \mu\text{m}$ ), as well as TPU/MWCNT nanocomposites of 1.0 wt.%, 2.5 wt.% and 5.0 wt.% from the compression moulding as well as FDM 3D printing process were measured (Figure 1c).

Experimental details and full description of the method to contact the sample, measurement of the temperature gradient ( $\Delta T$ ) the samples were exposed to, etc., have been previously reported [31,32]. In brief, the different samples were exposed to a temperature gradient stage where one block was maintained at room temperature ( $\sim 298$  K), while the other one was heated up to 373 K using a heating controller in 10 K steps. The generated thermoelectric voltage ( $\Delta V$ ) was measured with previously deposited metallic contacts using a digital multimeter (DMM) voltmeter (Agilent 34401A6 $\frac{1}{2}$ , Agilent, Santa Clara, CA, USA), capable of data logging to a PC. K-type thermocouples were placed onto the two blocks to continuously measure the temperature and precisely determine thus the temperature gradient,  $\Delta T$ . The Seebeck coefficient was derived then from  $\Delta V$  vs.  $\Delta T$  curve's slope by linear fitting. The Agilent 34401A6 $\frac{1}{2}$  DMM that was employed in this work was operated in the measurement range of 100 mV which gives a maximum resolution of 100 nV in this range. Moreover, according to the manufacturer specifications, the measurement accuracy/error in this range is  $\pm 8.5$   $\mu$ V (1 Year DMM operating at  $23 \pm 5$   $^{\circ}$ C; the temperature of the environment that all the measurements have been performed in our study).

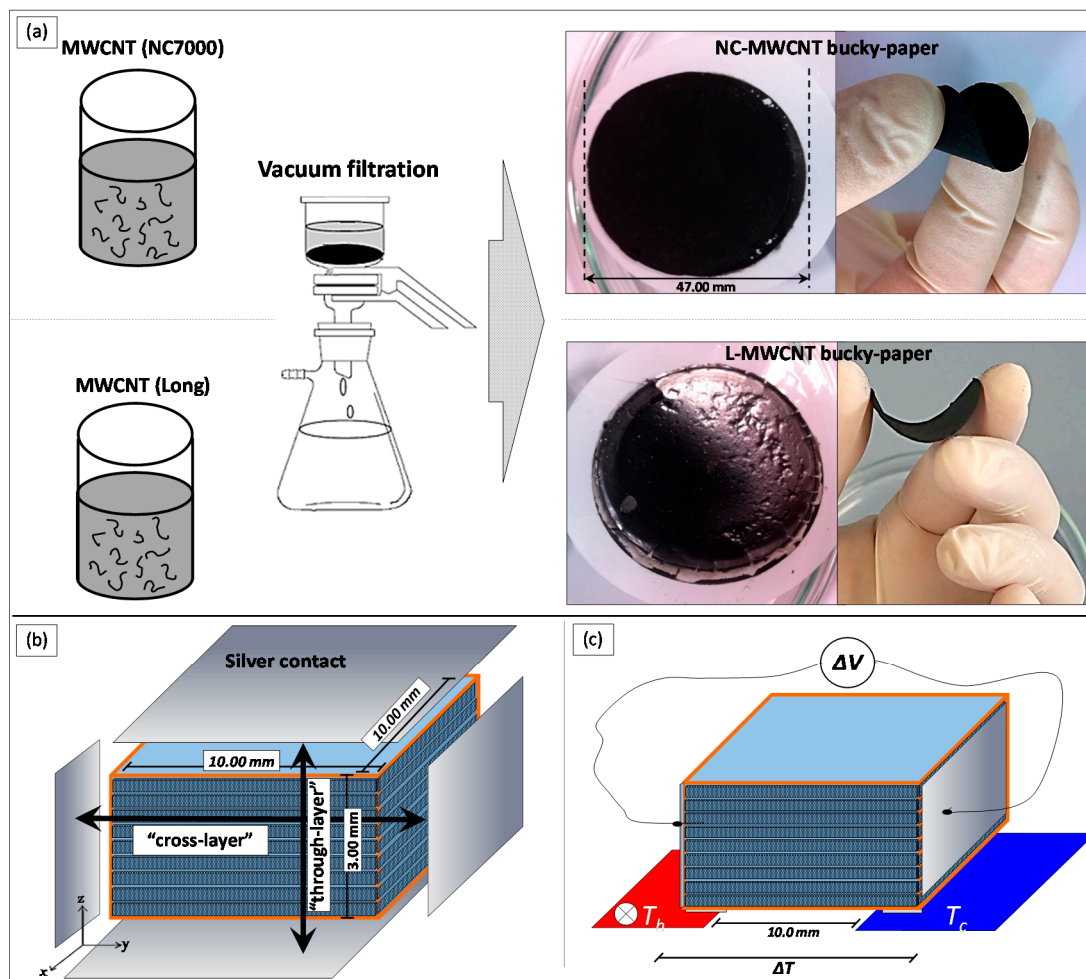


**Figure 1.** (a) Vacuum filtration process to fabricate MWCNT bucky paper films. (b) Schematic illustration of the cross- and through-layer electrical conductivity measurements for the different TPU/MWCNT FDM 3D printed nanocomposites, and (c) thermal gradient set-up used for the Seebeck coefficient measurements.

For the thermal conductivity measurements performed at room temperature, samples with a disk geometry of 12.5 mm diameter and 2 mm thickness were required. The Netzsch LFA 447 Nano Flash (Netzsch equipment manufacturing GmbH, Selb, Germany) thermal conductivity commercial

measurement set-up was used to study the thermal conductivity of all TPU/MWCNT nanocomposites. Circular plates of 12.5 mm and a thickness of 2 mm were prepared using hot-press in a similar manner as for the electrical conductivity measurements described above. The through-thickness (through-layer) thermal conductivity of 3D printed nanocomposites was measured also on 3D printed TPU/MWCNT nanocomposite samples with a diameter of 12.5 mm and a thickness of 2 mm.

Tensile test experiments of the nanocomposite samples prepared by compression moulding from the precursor filaments and 3D printed samples were carried out at room temperature using a Universal Testing Machine with a crosshead speed of 5 mm/s. As similarly reported in another study, rectangular and not dog-bone shaped samples (dimensions: 1.6 mm (width)  $\times$  1.6 mm (thickness)  $\times$  100 mm (length)) were tested in order to avoid possible stress concentration points that could be possibly created in the curvatures of a typical dog-bone sample with discrete lines [8].

### 3. Results and Discussion

#### 3.1. Raman Analysis and Electrical Conductivity of NC-MWCNT and L-MWCNT

Figure 2 shows the Raman spectrum of NC-MWCNT and L-MWCNT, respectively, in the spectral region of 900–3000  $\text{cm}^{-1}$ . In order to appropriately define the Lorentzian D- and G-peaks' characteristics of the Raman spectra, a curve fitting analysis was performed. Namely, the G- and D-band peaks were centred at 1565 and 1345  $\text{cm}^{-1}$  and these signals are characteristic of CNTs [33]. It is worth mentioning that radial breathing mode (RBM) peaks at, i.e., 100–300  $\text{cm}^{-1}$ , were absent, indicating that the CNTs were of multiwalled (MWCNTs) type rather than single-wall carbon nanotubes (SWCNTs). Additionally, the detection of the 2D band also confirms that the nanotubes are of MWCNT type [16]. In the spectra, two distinct spectral regions can be observed: one at 1000 and 2000  $\text{cm}^{-1}$  and the second one between 2300 and 3000  $\text{cm}^{-1}$ . The first one is governed by two broad bands, namely the G-band (G stands for “graphitic”) between 1500 and 1600  $\text{cm}^{-1}$ , and the D-band (D stands for “defects” or disorder) at 1300–1400  $\text{cm}^{-1}$ , which results from a disorder-induced double resonant process due to the breakdown of the usual wave vector selection rule ( $A_{1g}$  symmetry) [34]. In the second-order region, three main bands between 2300 and 3000  $\text{cm}^{-1}$  could be observed, i.e., the (T + D)D' (2450  $\text{cm}^{-1}$ ), 2D (2675  $\text{cm}^{-1}$ ) and the G + D (2900  $\text{cm}^{-1}$ ), which are assigned to overtones and combinations of the bands arising from the first order region. The graphitization and degree of crystallinity of CNTs have been several times correlated to the relative intensity ratio of the corresponding D and G-bands ( $I_D/I_G$ ) as a well-established indicator [35]. Specifically, the D and G band intensity ratio ( $I_D/I_G$ ) decreases from 1.33 for NC-MWCNT to 0.57 for L-MWCNT. This can be explained by a larger number of defects and existing  $sp^3$ -hybridized carbons in the nanotube framework, which may affect further the MWCNT charge carrier transport properties responsible for both the electrical conductivity and thermoelectric properties. The inherent electrical conductivity of NC-MWCNT and L-MWCNT measured with a four-point probe method on bucky paper films revealed an electrical conductivity of  $1.6 \times 10^3$  S/m for NC-MWCNT and  $8.4 \times 10^3$  S/m for L-MWCNT. This is more precisely attributed to the higher graphitic nature of L-MWCNT compared to NC-MWCNT shown by the Raman analysis.

#### 3.2. Morphological Analysis of NC-MWCNT and L-MWCNT

SEM analysis showed distinct differences of the NC-MWCNT (Figure 3a) as compared to the L-MWCNT (Figure 3b), investigated by the corresponding CNT bucky paper films. In both cases, highly entangled CNTs can be observed characteristic of bucky paper film morphology. The NC-MWCNT exhibit in general shorter lengths as well as an apparent tendency to curve in their main axis. On the other hand, the L-MWCNT exhibit quite high CNT lengths, which directly affects the CNT aspect ratio known to be an important parameter for the CNT electrical transport properties as well as affecting the electrical percolation threshold and the induced bulk conductivity polymer/CNT nanocomposites.

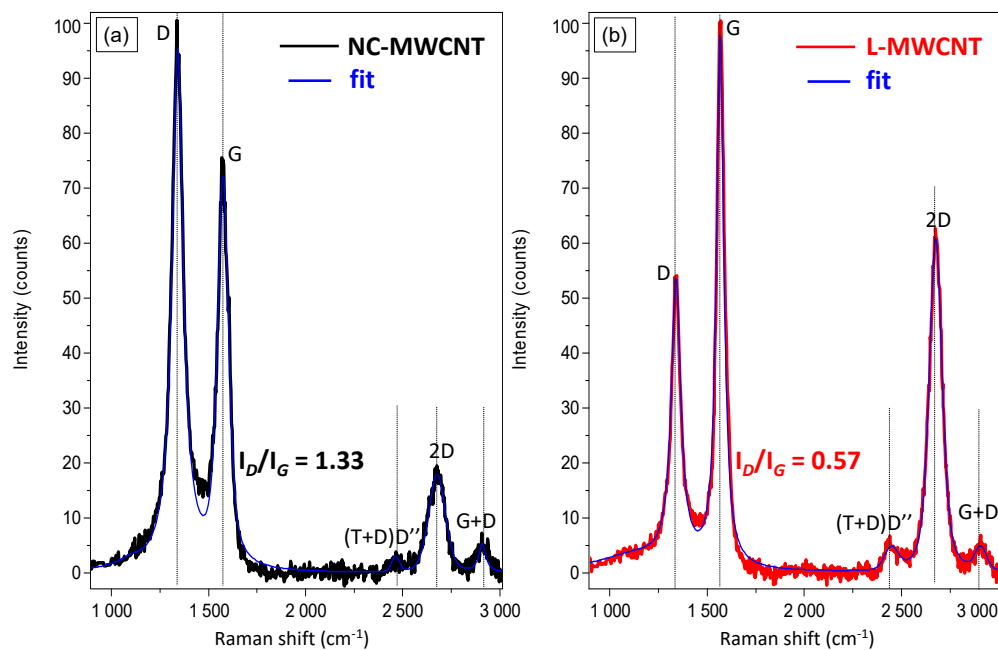


**Figure 2.** Raman spectra of (a) NC-MWCNT and (b) L-MWCNT showing characteristic bands of MWCNT material with different graphitization degree and number of defects of the CNT graphitic lattice.

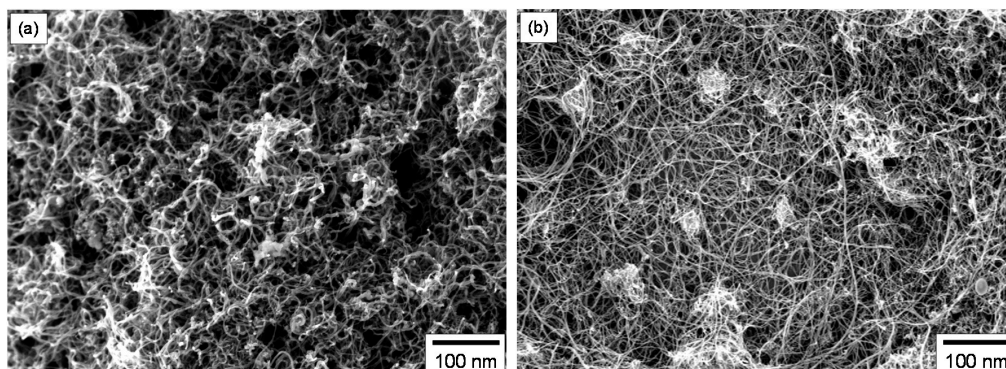


**Figure 3.** SEM images of bucky paper films consisting of (a) NC-MWCNT and (b) L-MWCNT.

### 3.3. Microstructure Investigations of the FDM 3D Printed TPU/MWCNT Nanocomposites

The SEM and TEM images of 3D printed TPU/MWCNT nanocomposites of 2.5 wt.% MWCNT content could be seen in Figure 4. The SEM images were acquired from cryo-fractured surfaces of FDM 3D printed samples broken perpendicular to the Y-printing direction, while crosssections for the TEM analysis were also obtained from sample's broken "block-surface" perpendicular to the Y-printing direction. Figure 4a shows the SEM surface morphology of TPU/NC-MWCNT, while Figure 4b shows the morphology of TPU/L-MWCNT. In both cases, a homogeneous distribution of CNTs in the TPU polymer matrix could be observed with quite rough surfaces and visible CNTs due to the fracture process. In general the TPU/L-MWCNT exhibits much higher roughness compared to TPU/NC-MWCNT, possibly due to the longer CNT lengths that some are pulled out from the polymer matrix upon the destructive cryofracture process. Moreover, a highly entangled CNT network could be observed endowing the electrical and thermoelectric properties to the TPU/MWCNT nanocomposites. Figure 4c illustrates the TEM image of TPU/NC-MWCNT nanocomposite, while Figure 4d shows that of TPU/L-MWCNT. The TEM images reveal the MWCNT nanodispersion status, while both NC-MWCNTs and L-MWCNTs do not form any primary as well as secondary agglomerates. MWCNTs have been sufficiently disentangled in both cases with single dispersed nanotubes observed within the TPU matrix creating a high quality of geometrically percolated CNT network. This is attributed

to the excessive infiltration of the CNT clusters by the TPU polymer melt and the shear forces during melt mixing resulting in highly dispersed CNT nanofillers, desired for the optimum electrical conductivity of the final nanocomposites. The high quality and dispersion of MWCNTs within the TPU polymer matrix would allow enhanced electrical conductivity and mechanical properties of the final nanocomposites [36]. Furthermore, it is critical that a high quality of CNT dispersion has been observed within the TPU/MWCNT nanocomposites, since the existence of micro-aggregates can cause nozzle clogging and affect the final 3D printed object's quality.

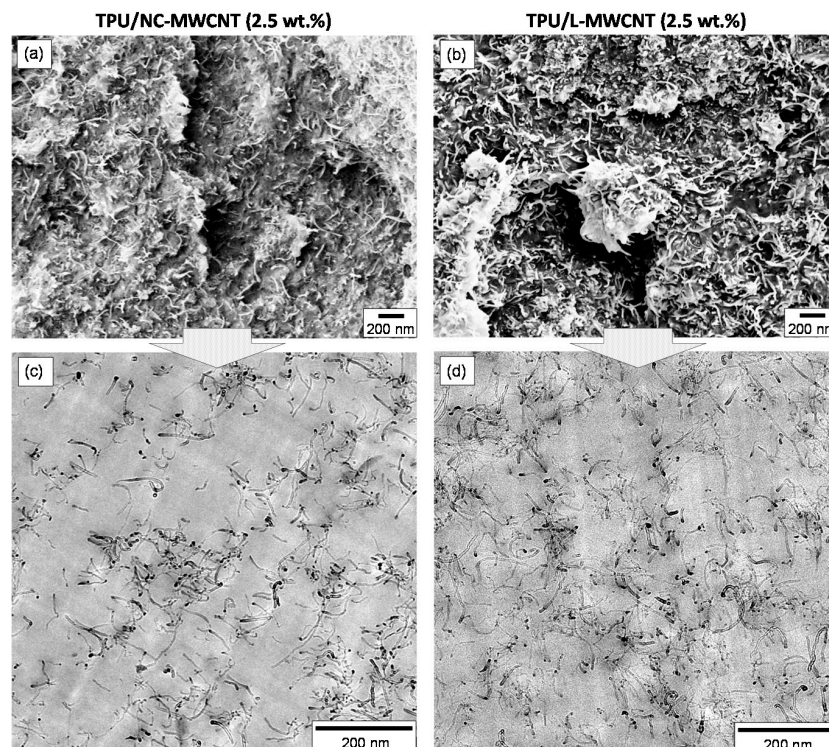


**Figure 4.** (a,b) SEM images of the 3D printed TPU/NC-MWCNT (2.5 wt.%) and TPU/L-MWCNT (2.5 wt.%) fractured surfaces, respectively. (c) TEM images of the TPU/NC-MWCNT (2.5 wt.%) and (d) TPU/L-MWCNT (2.5 wt.%) nanocomposites showing the achieved CNT nanodispersion in the TPU matrix.

### 3.4. Mechanical Properties

Table 1 summarizes the measured modulus, tensile strength and elongation at break of the extruded neat TPU, TPU/NC-MWCNT and TPU/L-MWCNT at 1.0 wt.%, 2.5 wt.% and 5.0 wt.% loadings, as well as 3D printed TPU, TPU/NC-MWCNT and TPU/L-MWCNT with the same filler loading. For all samples, the initial 10% strain region was used in order to calculate the respective moduli, where the stress–strain relationship was linear. In general, the strength of both the TPU-extruded filaments and the FDM 3D printed ones increased with the addition of MWCNTs, being in good agreement with a review that can be found in the literature [37]. On the other hand, the modulus has been slightly decreased after 3D printing. On average, a decrease of ~11.9% has been calculated comparing the moduli of the filament derived compression moulded samples with the corresponding FDM 3D printed ones. This is obviously superior to what has been already reported in the literature for 3D printed ABS samples compared to bulk ABS [3]. Another important finding to point out is a slight decrease in the strength of all the fabricated FDM 3D printed samples, compared to their respective filament counterparts. This is due to the FDM additive manufacturing 3D printing process resulting into small interlayer voids, as well as plausibly interfacial weak and/or imperfect interlayer bonding as has been reported in several studies [8]. It is also worth mentioning that the 3D printed TPU/NC-MWCNT and



TPU/L-MWCNT nanocomposites with the maximum MWCNT content (5.0 wt.%) could be strained only up to 118% and 129%, respectively. This low-strain failure can be ascribed to the weak adhesion between the 3D sample layers or to existing CNT micro-aggregates in such high filler loading that may act as “defects” and/or stress concentration points within the material decreasing significantly the % elongation at break and tensile strength. Subsequently, (i) more possible defects and (ii) weak interfacial strength of the interlayer bonds could act as stress concentration locations, causing the 5 wt.% filled samples to fail at lower strains. Figure 5 shows, representatively, the stress–strain curves of all 3D printed samples, namely the TPU, TPU/NC-MWCNT and TPU/L-MWCNT nanocomposites at 1.0 wt.%, 2.5 wt.% and 5.0 wt.% MWCNT loadings. On one hand, the TPU/L-MWCNT nanocomposites depict a more prominent increase of the moduli as well as of the tensile strength for all the MWCNT filler loadings compared to the TPU/NC-MWCNT (short CNTs). This is attributed to the higher aspect ratio and length of L-MWCNTs as well as the higher graphitic nature possible affecting the inherent mechanical properties of CNTs. On the other hand, the tensile strength of all TPU/MWCNT nanocomposites is increased with the addition of 1.0 wt.% MWCNTs, while showing a decrease for 2.5 and 5.0 wt.% of MWCNT loadings.

**Table 1.** Modulus, tensile strength and elongation at break of the extruded TPU, TPU/NC-MWCNT and TPU/L-MWCNT as well as 3D printed TPU, TPU/NC-MWCNT and TPU/L-MWCNT nanocomposites.

Sample.	E-Modulus (MPa)	Tensile Strength (MPa)	Elongation at Break (%)
TPU	10.28 ± 1.22	33.78 ± 1.34	612
3D printed TPU	7.96 ± 1.67	32.12 ± 1.16	601
TPU/NC-MWCNT (1.0 wt.%)	17.56 ± 1.25	28.54 ± 1.84	632
3D TPU/NC-MWCNT (1.0 wt.%)	14.85 ± 1.13	27.86 ± 1.92	625
TPU/NC-MWCNT (2.5 wt.%)	22.32 ± 2.33	22.65 ± 1.32	575
3D TPU/NC-MWCNT (2.5 wt.%)	20.08 ± 2.84	21.08 ± 1.97	530
TPU/NC-MWCNT (5.0 wt.%)	25.01 ± 2.55	9.55 ± 1.12	154
3D TPU/NC-MWCNT (5.0 wt.%)	24.13 ± 2.98	5.85 ± 2.02	118
TPU/L-MWCNT (1.0 wt.%)	19.84 ± 1.12	29.35 ± 1.74	644
3D TPU/L-MWCNT (1.0 wt.%)	16.54 ± 1.26	28.13 ± 1.45	637
TPU/L-MWCNT (2.5 wt.%)	24.52 ± 2.86	24.86 ± 1.56	602
3D TPU/L-MWCNT (2.5 wt.%)	22.34 ± 2.49	23.54 ± 1.23	558
TPU/L-MWCNT (5.0 wt.%)	28.56 ± 3.95	10.45 ± 0.98	161
3D TPU/L-MWCNT (5.0 wt.%)	26.67 ± 3.44	6.48 ± 1.14	129

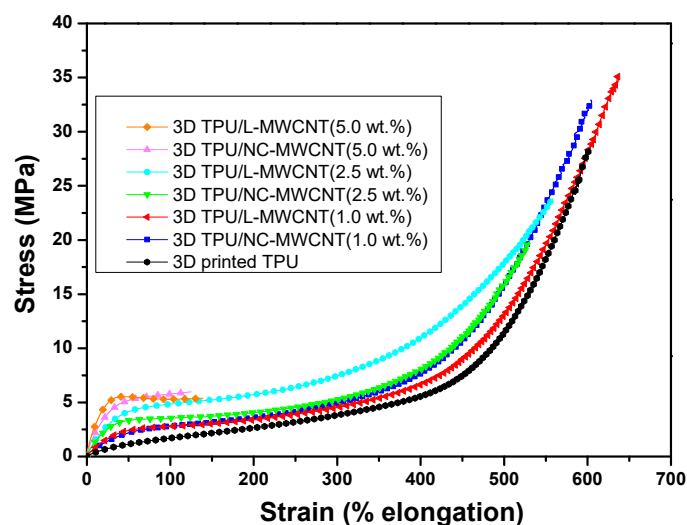


**Figure 5.** Stress–strain curves of all 3D printed samples, namely TPU, TPU/NC-MWCNT and TPU/L-MWCNT nanocomposites at 1.0, 2.5 and 5.0 wt.% MWCNT loadings.

### 3.5. Electrical Conductivity of TPU/MWCNT Nanocomposites

Figure 6a shows the in-plane electrical conductivity of TPU/NC-MWCNT and TPU/L-MWCNT thermal-pressed nanocomposites at 1.0, 2.5 and 5.0 wt.% MWCNT content. The highest conductivities were determined for the 5.0 wt.% TPU/MWCNT nanocomposites, namely 45.2 S/m (TPU/NC-MWCNT) and 94.1 S/m (TPU/L-MWCNT). It should be noted that the electrical conductivities of NC-MWCNT was  $1.6 \times 10^3$  S/m, while for the L-MWCNT  $8.4 \times 10^3$  S/m. This reveals that the resulting TPU/MWCNT nanocomposites reached two orders of magnitude lower electrical conductivity values at 5.0 wt.% MWCNT content, as compared to the inherent electrical conductivity of the MWCNTs used in each case as the electrically conductive filler. The higher conductivity of TPU/L-MWCNT at all MWCNT contents may be attributed to two factors: (i) due to the inherently higher electrical conductivity of L-MWCNTs and (ii) due to the aspect ratio of the filler that has been reported to strongly affect the percolation threshold as well as the electrical conductivity of the resulting CPCs [38,39]. Figure 6b shows the electrical conductivity of the 3D printed TPU/MWCNT nanocomposites at 1.0, 2.5 and 5.0 wt.% MWCNT contents at two different measurement directions, namely the “through layer” or through thickness as we as the “cross-layer” or in-plane of the 3D printed object. As it can be observed, the electrical conductivity values were in the same range as for the pressed ones showing that the conductivity of TPU/MWCNT nanocomposites was well maintained in both directions after the FDM printing. However, the scattering of the values, indicated by the corresponding standard deviations, was a bit higher compared to the compression moulded ones due to possibly more inhomogeneities of the 3D printed samples. It is also interesting to mention that for all 3D printed TPU/NC-MWCNT and TPU/L-MWCNT nanocomposites at different MWCNT contents, the cross layer conductivity values were a bit higher than the through layer ones most likely attributed to the FDM 3D printing process endowing thus an “anisotropic” character of the electrical properties of the final nanocomposites. More precisely, a plausible explanation for the slightly higher electrical conductivity in the cross layer direction could be that the printing process induces some extent of CNT orientation in the print deposition direction, resulting thus in a slightly better “bulk” electrical conductivity. This finding has been also observed and reported in a previous study for 3D printed CPCs [8].

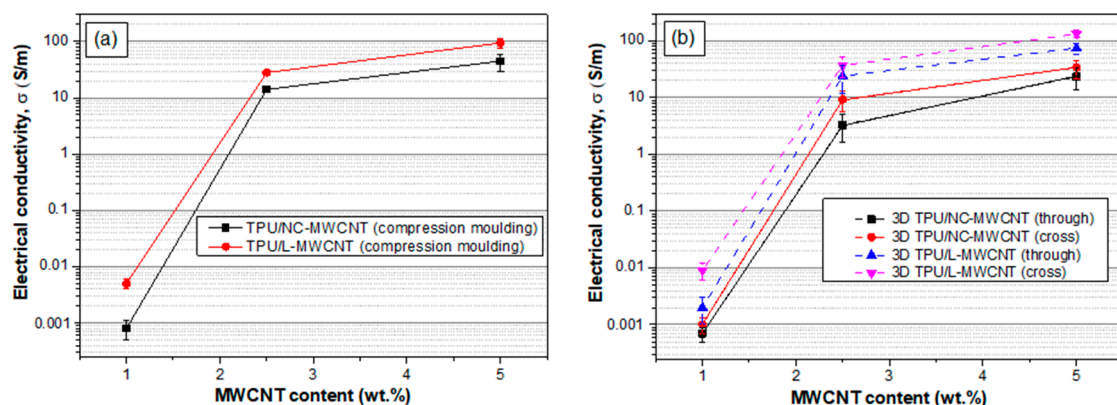


**Figure 6.** (a) Electrical conductivity of TPU/NC-MWCNT and TPU/L-MWCNT thermal-pressed nanocomposites at 1.0, 2.5 and 5.0 wt.% MWCNT content (at “in-plane” direction of the compression moulded films). (b) Electrical conductivity of the 3D printed TPU/MWCNT nanocomposites at 1.0, 2.5 and 5.0 wt.% MWCNT contents at “through layer” and “cross-layer” printing directions.

### 3.6. Seebeck Coefficient (S), Power Factor (PF) and Thermoelectric Figure of Merit (ZT) of TPU/MWCNT Nanocomposites

Figure 7 presents the Seebeck coefficient, power factor (PF) and thermoelectric figure of the merit (ZT)-derived values of the compression moulded as well as the 3D printed TPU/MWCNT nanocomposites at 1.0, 2.5 and 5.0 wt.% MWCNT content. Specifically, Figure 7a demonstrates the Seebeck coefficient of TPU/NC-MWCNT and TPU/L-MWCNT nanocomposites prepared by

compression moulding of the corresponding precursor filaments. The Seebeck coefficient for both pressed and 3D printed TPU/NC-MWCNT nanocomposites was in the range of 8.0–8.5  $\mu\text{V/K}$  with a tendency to slightly increase from the 1.0 to 5.0 wt.% reaching  $\sim 8.5 \mu\text{V/K}$ , as the sample showed a higher CNT content and getting far from the percolation threshold. On the other hand, the Seebeck coefficient for both pressed and 3D printed TPU/L-MWCNT nanocomposites was much higher, namely in the range of 18.0–18.5  $\mu\text{V/K}$ . The Seebeck coefficient of the NC-MWCNT and L-MWCNT measured in the bucky paper form were  $9.2 \pm 0.3$  and  $19.8 \pm 0.2 \mu\text{V/K}$ , respectively. It should be noted herein that the thermoelectric property which arises from the CNT material is endowed to the respective TPU/MWCNT nanocomposites; while it is being preserved through all the different melt-mixing, compression moulding and 3D printing processes.

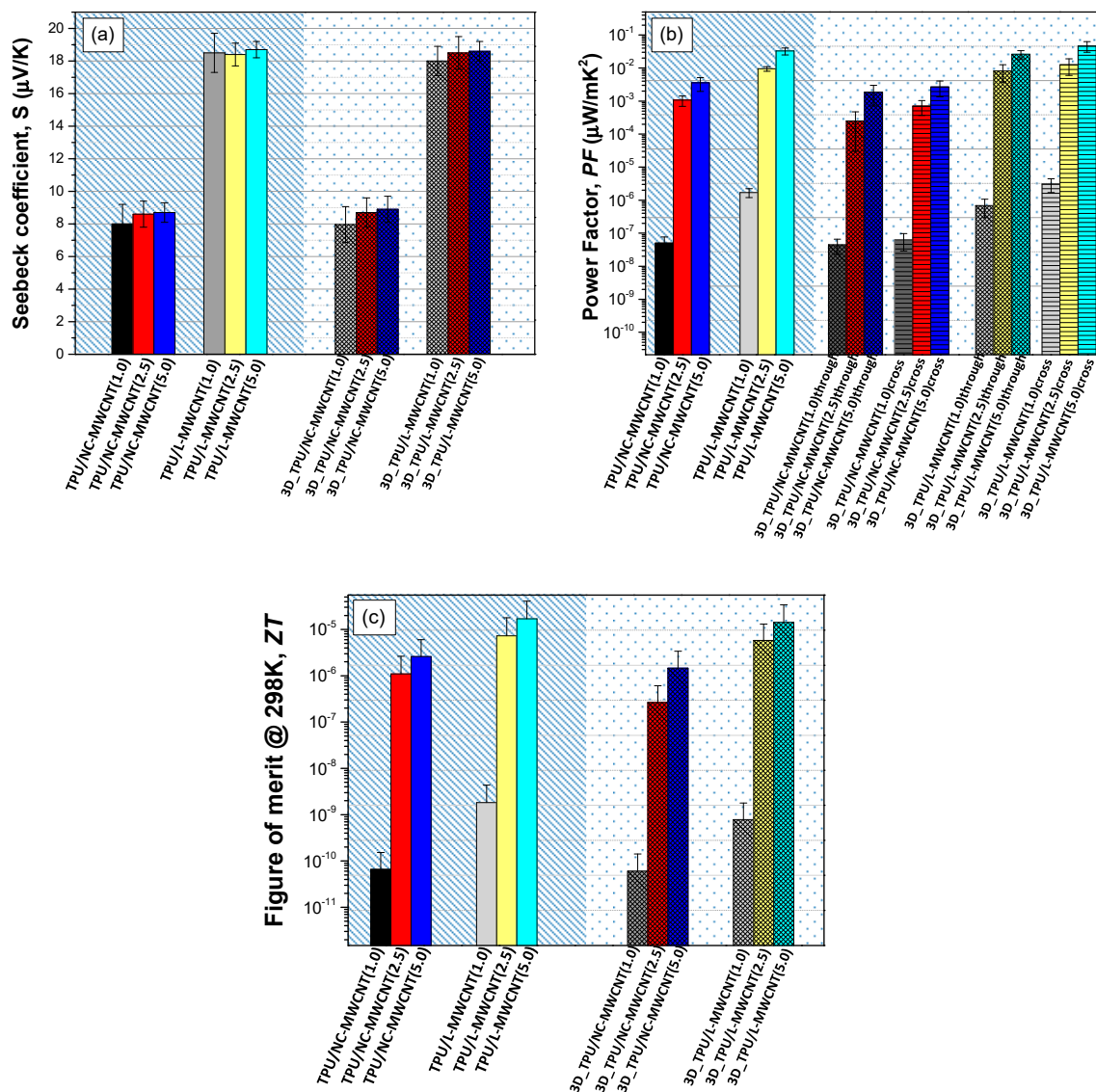


**Figure 7.** (a) Seebeck coefficient of TPU/NC-MWCNT and TPU/L-MWCNT nanocomposites prepared by compression moulding of the corresponding precursor filaments, and (b)  $PF$  values of the compression moulded as well as the 3D printed TPU/MWCNT nanocomposites at 1.0, 2.5 and 5.0 wt.% MWCNT content, considering the through- and cross-layer-measured electrical conductivities (Seebeck coefficient arising only from the CNT material is the same in all measured directions since it is an inherent property of the NW- and L-MWCNTs, respectively), (c) Figure of merit ( $ZT$ ) of the compression moulded, as well as the 3D printed TPU/MWCNT nanocomposites (1.0, 2.5 and 5.0 wt.% MWCNT content).

Figure 7b demonstrates the  $PF$  values of the compression moulded as well as the 3D printed TPU/MWCNT nanocomposites at 1.0, 2.5 and 5.0 wt.% MWCNT content, considering the through layer and cross-layer-measured electrical conductivities. It can be seen that the  $PF$  values increase in general by increasing the CNT content in all CPCs, while this is due only to the increase in the nanocomposite's electrical conductivity at higher CNT loadings. Moreover, the  $PF$  values are higher for the TPU/L-MWCNT nanocomposites compared to the TPU/NC-MWCNT ones, due to both the higher electrical conductivity and Seebeck coefficient values. An interesting point also to be figured out is the anisotropic thermoelectric behaviour of the 3D printed TPU/NC-MWCNT and TPU/L-MWCNT nanocomposites at different MWCNT contents for the through- and cross-layer directions. For both TPU/NC-MWCNT and TPU/L-MWCNT nanocomposites, the derived  $PF$  values are slightly higher for the cross-layer directions attributed only to the higher electrical conductivity in cross-layer that has been determined and discussed previously. Namely, the highest  $PF$  value was found for the 3D printed TPU/L-MWCNT nanocomposite at 5.0 wt.% CNT content ( $PF = 0.02 \mu\text{W}/\text{mK}^2$  and  $0.04 \mu\text{W}/\text{mK}^2$  for through layer and cross-layer direction, respectively).

CNT-based polymer nanocomposites with non-conductive engineered polymers (thermoplastics, thermosets, elastomer), as well as with conductive conjugated polymer matrices, have been reported several times until now, while TEG devices have been fabricated also using serially interconnected polymer nanocomposite thermocouples [40]. Namely, solvent-mixed single-walled carbon nanotubes (SWCNTs) with relatively high filler loadings ( $>>50$  wt.%) in poly (3,4-ethylenedioxythiophene): poly (styrene sulfonate) (PEDOT:PSS) have reached the highest ever reported  $PF$  value of  $140 \mu\text{W}/\text{mK}^2$  amongst polymer/CNT nanocomposites [41]. However, the low thermal stability and hygroscopic nature of PEDOT:PSS is an obstacle to various applications. Engineered and high temperature resistance thermoplastic polyetherimide (PEI)/SWCNT nanocomposites prepared by solvent mixing have been previously reported by our group, reaching a  $PF$  of  $3.7 \times 10^{-2} \mu\text{W}/\text{mK}^2$  at 10.0 vol% of SWCNTs [21]. Polycarbonate/MWCNT melt-mixed nanocomposites have been also reported with  $PF$  of  $\sim 8 \times 10^{-4} \mu\text{W}/\text{mK}^2$  at 2.5 wt.% MWCNT loading [42]. In another study, Polypropylene-based melt-mixed composites with fixed SWCNT (2 wt.%) and copper oxide (5 wt.%) showed that using a low-molecular weight polyethylene glycol (PEG) during melt mixing as a process additive, p-type composites switched into n-type while the highest  $PF$  value achieved was in the range of  $\sim 5 \times 10^{-3} \mu\text{W}/\text{mK}^2$  [40]. To the best of the authors' knowledge, it could be realised that, in this research work, the highest ever reported value of  $PF$  has been achieved for melt-mixed and 3D printable/processed TPU/L-MWCNT stretchable nanocomposites at 5.0 wt.% of MWCNT content ( $0.02$  and  $0.04 \mu\text{W}/\text{mK}^2$  for through- and cross-layer directions). The  $PF$  values are slightly lower than our previously reported solvent mixed PEI/SWCNT nanocomposites at 10 vol.% SWCNT content mentioned above ( $PF = 3.7 \times 10^{-2} \mu\text{W}/\text{mK}^2$ ) [21].

Figure 7c summarizes the dimensionless thermoelectric figure of merit ( $ZT$ ) of the compression-moulded, as well as the 3D printed TPU/MWCNT nanocomposites at 1.0, 2.5 and 5.0 wt.% MWCNT content, as a well-known measure to determine the materials' thermoelectric efficiency ( $ZT$ ;  $ZT = \frac{\sigma \times S^2}{\kappa} T = \frac{PF}{\kappa} T$ ,  $\kappa$  is the thermal conductivity,  $PF$  the power factor, and  $T$  the absolute temperature) [26]. For the calculation of the 3D printed nanocomposite's  $ZT$ , it is worth mentioning that the "through layer"  $PF$  values were used to derive the corresponding  $ZT$  presented values. Specifically, the  $ZT$  values increase with increased CNT content in all CPCs. Moreover, the  $ZT$  values are higher for the TPU/L-MWCNT nanocomposites compared to the TPU/NC-MWCNT ones, due to higher  $PF$  values with slight variations in the thermal conductivity values (Table 2). Namely, the highest  $ZT$  values were found for the TPU/L-MWCNT nanocomposite at 5.0 wt.% CNT content ( $ZT = 1.42 \times 10^{-5}$  and  $1.69 \times 10^{-5}$  for the compression moulding and the 3D printed fabricated nanocomposite, respectively).

The thermal conductivity of the TPU/CNT nanocomposites is shown in Table 2. As it can be observed, all samples exhibited relatively low thermal conductivity values, i.e., in the range of  $0.22$ – $0.55 \text{ W}/\text{mK}$  [43] with slight increase with the increased CNT filler loading. It is worth mentioning that the low thermal conductivity of the nanocomposites is an important characteristic for the

utilization of the TPU/MWCNT CPC nanocomposites as efficient thermoelectric materials, due to their ability to sustain a temperature difference upon being exposed to a temperature gradient ( $\Delta T$ ). Therefore, the sustained temperature gradient within the material is the driving force for the thermoelectrically generated charge carriers. The thermal conductivity values are in accordance with the previously reported melt-mixed PC/MWCNT CPC materials, where it has been shown that the thermal conductivity remains below  $0.6 \text{ W/m K}^{-1}$  even at 15 wt.% of MWCNT filler content. Overall, it should be made clear that the  $ZT$  for such CPC nanocomposites has to be significantly increased in the future, i.e., by at least two orders of magnitude, in order to enable the commercialization of the proposed materials and fabrication of thermoelectric generator (TEG) power-generating devices made thereof. It is expected that melt-mixed thermoplastics with (i) higher CNT loadings, and (ii) the use of differently functionalized/doped CNTs, focusing mainly on SWCNTs that are more conductive materials, could be promising approaches to increase the electrical conductivity, as well as the Seebeck coefficient of the resulting CPCs towards highly efficient polymer/CNT organic thermoelectrics.

**Table 2.** Thermal conductivity of the extruded TPU, TPU/NC-MWCNT and TPU/L-MWCNT as well as 3D printed TPU, TPU/NC-MWCNT and TPU/L-MWCNT nanocomposites (at 1.0, 2.5 and 5.0 wt.% filler content).

Sample	Thermal Conductivity, $\kappa$ (W/m K)
TPU	$0.20 \pm 0.01$
3D printed TPU	$0.19 \pm 0.02$
TPU/NC-MWCNT (1.0 wt.%)	$0.23 \pm 0.02$
3D TPU/NC-MWCNT (1.0 wt.%)	$0.22 \pm 0.01$
TPU/NC-MWCNT (2.5 wt.%)	$0.29 \pm 0.02$
3D TPU/NC-MWCNT (2.5 wt.%)	$0.28 \pm 0.01$
TPU/NC-MWCNT (5.0 wt.%)	$0.41 \pm 0.04$
3D TPU/NC-MWCNT (5.0 wt.%)	$0.38 \pm 0.02$
TPU/L-MWCNT (1.0 wt.%)	$0.28 \pm 0.02$
3D TPU/L-MWCNT (1.0 wt.%)	$0.26 \pm 0.01$
TPU/L-MWCNT (2.5 wt.%)	$0.39 \pm 0.03$
3D TPU/L-MWCNT (2.5 wt.%)	$0.42 \pm 0.02$
TPU/L-MWCNT (5.0 wt.%)	$0.58 \pm 0.04$
3D TPU/L-MWCNT (5.0 wt.%)	$0.55 \pm 0.02$

#### 4. Conclusions

3D printed thermoelectric polymer nanocomposite materials that can be also flexible and stretchable have been fabricated for the first time and fully characterised in the study at hand. An optimised process of combined melt-mixing compounding and extrusion was developed for the fabrication of 3D printable TPU/MWCNT nanocomposite filaments with 1.0, 2.5 and 5.0 wt.% CNT contents, while two different types of commercially available CNTs with significant differences in morphology, electrical and thermoelectric properties have been utilised. The 3D printed TPU/MWCNT nanocomposite samples exhibited an anisotropic electrical conductivity in the through- and cross-layer printing direction, while no difference in the Seebeck coefficient since it is an inherent material property arising from the CNT type. The 3D printed TPU/MWCNT thermoelements can be the building blocks for the fabrication of flexible and stretchable organic thermoelectric generators (TEGs) by 3D printing FDM technology combined with an ink-jet printer head for the fabrication of the metallic contacts required as junctions for the serial interconnection of the thermoelements. The 3D printed thermoelectric TPU/MWCNT materials could open new avenues towards large-scale thermal energy-harvesting applications, i.e., wearables, stretchable 3D shaped harvesters, etc., where complex 3D architectures and customizability are required.

**Author Contributions:** L.T. contributed to the preparation of the TPU/CNT nanocomposite filaments. L.T., M.P., S.G. and N.V. contributed equally to the conceptualization of the whole work. L.T., M.P., S.G. and N.V. designed the experimental campaign as well as all methods performed and techniques used in this work. L.T., M.P., S.G. designed the methodology as well as the manufacturing/processing parameters of the TPU/CNT conductive nanocomposites. L.T., M.P. and S.G. contributed in the analysis and interpretation of the morphological, mechanical, electric and thermoelectric properties data. L.T., M.P. wrote the first draft of the paper. L.T. performed all the electrical and thermoelectric measurements, as well as the SEM and TEM investigations (SEM and TEM) in this study. L.T., M.P., S.G. and N.V. coordinated the mentioned activities. The manuscript was written through contributions of all authors. All authors have read and agreed to the published version of the manuscript.

**Funding:** This research received no external funding.

**Acknowledgments:** L.T. gratefully acknowledges the Bodossaki Foundation for financial support in the framework of institutional scholarships.

**Conflicts of Interest:** The authors declare no conflict of interest. The funding sponsors had no role in the design of the study; in the collection, analyses, or interpretation of data; in the writing of the manuscript, and in the decision to publish the results.

## References

1. Takagishi, K.; Umez, S. Development of the Improving Process for the 3D Printed Structure. *Sci. Rep.* **2017**, *7*, 39852. [[CrossRef](#)] [[PubMed](#)]
2. Lewicki, J.P.; Rodriguez, J.N.; Zhu, C.; Worsley, M.A.; Wu, A.S.; Kanarska, Y.; Horn, J.D.; Duoss, E.B.; Ortega, J.M.; Elmer, W.; et al. 3D-Printing of Meso-structurally Ordered Carbon Fiber/Polymer Composites with Unprecedented Orthotropic Physical Properties. *Sci. Rep.* **2017**, *7*, 43401. [[CrossRef](#)] [[PubMed](#)]
3. Vidakis, N.; Maniadi, A.; Petousis, M.; Vamvakaki, M.; Kenanakis, G.; Koudoumas, E. Mechanical and Electrical Properties Investigation of 3D-Printed Acrylonitrile–Butadiene–Styrene Graphene and Carbon Nanocomposites. *J. Mater. Eng. Perform.* **2020**, *29*, 1909–1918. [[CrossRef](#)]
4. Taylor, A.P.; Cuervo, C.V.; Arnold, D.P.; Velásquez-García, L.F. Fully 3D-Printed, Monolithic, Mini Magnetic Actuators for Low-Cost, Compact Systems. *J. Microelectromechanical Syst.* **2019**, *28*, 481–493. [[CrossRef](#)]
5. Le, T.; Song, B.; Liu, Q.; Bahr, R.A.; Moscato, S.; Wong, C.; Tentzeris, M.M. A novel strain sensor based on 3D printing technology and 3D antenna design. In Proceedings of the 2015 IEEE 65th Electronic Components and Technology Conference (ECTC), San Diego, CA, USA, 26–29 May 2015; pp. 981–986.
6. Tzounis, L.; Zappalorto, M.; Panozzo, F.; Tsirka, K.; Maragoni, L.; Paipetis, A.S.; Quaresimin, M. Highly conductive ultra-sensitive SWCNT-coated glass fiber reinforcements for laminate composites structural health monitoring. *Compos. Part B Eng.* **2019**, *169*, 37–44. [[CrossRef](#)]
7. Leigh, S.J.; Bradley, R.J.; Purssell, C.P.; Billson, D.R.; Hutchins, D.A. A Simple, Low-Cost Conductive Composite Material for 3D Printing of Electronic Sensors. *PLoS ONE* **2012**, *7*, e49365. [[CrossRef](#)]
8. Christ, J.F.; Aliheidari, N.; Ameli, A.; Pötschke, P. 3D printed highly elastic strain sensors of multiwalled carbon nanotube/thermoplastic polyurethane nanocomposites. *Mater. Des.* **2017**, *131*, 394–401. [[CrossRef](#)]
9. Jaksic, N.I.; Desai, P.D. Characterization of resistors created by fused filament fabrication using electrically-conductive filament. *Procedia Manuf.* **2018**, *17*, 37–44. [[CrossRef](#)]
10. Han, T.; Kundu, S.; Nag, A.; Xu, Y. 3D Printed Sensors for Biomedical Applications: A Review. *Sensors* **2019**, *19*, 1706. [[CrossRef](#)]
11. Haghiashtiani, G.; Habtour, E.; Park, S.-H.; Gardea, F.; McAlpine, M.C. 3D printed electrically-driven soft actuators. *Extrem. Mech. Lett.* **2018**, *21*, 1–8. [[CrossRef](#)]
12. Tzounis, L.; Gravalidis, C.; Vassiliadou, S.; Logothetidis, S. Fiber yarns/CNT hierarchical structures as thermoelectric generators. *Mater. Today Proc.* **2017**, *4*, 7070–7075. [[CrossRef](#)]
13. Madan, D.; Wang, Z.; Chen, A.; Juang, R.-C.; Keist, J.; Wright, P.K.; Evans, J.W. Enhanced Performance of Dispenser Printed MA n-type Bi<sub>2</sub>Te<sub>3</sub> Composite Thermoelectric Generators. *ACS Appl. Mater. Interfaces* **2012**, *4*, 6117–6124. [[CrossRef](#)] [[PubMed](#)]
14. Liang, D.; Yang, H.; Finefrock, S.W.; Wu, Y. Flexible Nanocrystal-Coated Glass Fibers for High-Performance Thermoelectric Energy Harvesting. *Nano Lett.* **2012**, *12*, 2140–2145. [[CrossRef](#)] [[PubMed](#)]
15. Srinivasan, B.; Berthebaud, D.; Mori, T. Is LiI a Potential Dopant Candidate to Enhance the Thermoelectric Performance in Sb-Free GeTe Systems? A Prelusive Study. *Energies* **2020**, *13*, 643. [[CrossRef](#)]

16. Tzounis, L.; Liebscher, M.; Fuge, R.; Leonhardt, A.; Mechtcherine, V. P- and n-type thermoelectric cement composites with CVD grown p- and n-doped carbon nanotubes: Demonstration of a structural thermoelectric generator. *Energy Build.* **2019**, *191*, 151–163. [[CrossRef](#)]
17. Tzounis, L. Synthesis and Processing of Thermoelectric Nanomaterials, Nanocomposites, and Devices. In *Nanomaterials Synthesis*; Beeran Pottathara, Y., Thomas, S., Kalarikkal, N., Grohens, Y., Kokol, V., Eds.; Elsevier: Amsterdam, The Netherlands, 2019; Chapter 9; pp. 295–336.
18. Piao, M.; Kim, G.; Kennedy, G.P.; Roth, S.; Dettlaff-Weglikowska, U. Thermoelectric properties of single walled carbon nanotube networks in polycarbonate matrix. *Phys. Status Solidi (b)* **2013**, *250*, 1468–1473. [[CrossRef](#)]
19. Piao, M.; Na, J.; Choi, J.; Kim, J.; Kennedy, G.P.; Kim, G.; Roth, S.; Dettlaff-Weglikowska, U. Increasing the thermoelectric power generated by composite films using chemically functionalized single-walled carbon nanotubes. *Carbon* **2013**, *62*, 430–437. [[CrossRef](#)]
20. Tzounis, L.; Liebscher, M.; Mäder, E.; Pötschke, P.; Stamm, M.; Logothetidis, S. Thermal energy harvesting for large-scale applications using MWCNT-grafted glass fibers and polycarbonate-MWCNT nanocomposites. *AIP Conf. Proc.* **2015**, *1646*, 138–148.
21. Tzounis, L.; Hegde, M.; Liebscher, M.; Dingemans, T.; Pötschke, P.; Paipetis, A.S.; Zafeiropoulos, N.E.; Stamm, M. All-aromatic SWCNT-Polyetherimide nanocomposites for thermal energy harvesting applications. *Compos. Sci. Technol.* **2018**, *156*, 158–165. [[CrossRef](#)]
22. Qu, D.; Huang, X.; Li, X.; Wang, H.; Chen, G. Annular flexible thermoelectric devices with integrated-module architecture. *npj Flex. Electron.* **2020**, *4*, 1–7. [[CrossRef](#)]
23. Zhang, T.; Wang, Z.; Srinivasan, B.; Wang, Z.; Zhang, J.; Li, K.; Boussard-Pledel, C.; Troles, J.; Bureau, B.; Wei, L. Ultraflexible Glassy Semiconductor Fibers for Thermal Sensing and Positioning. *ACS Appl. Mater. Interfaces* **2019**, *11*, 2441–2447. [[CrossRef](#)] [[PubMed](#)]
24. Gao, C.; Chen, G. Conducting polymer/carbon particle thermoelectric composites: Emerging green energy materials. *Compos. Sci. Technol.* **2016**, *124*, 52–70. [[CrossRef](#)]
25. Tzounis, L.; Bangeas, P.I.; Exadaktylos, A.; Petousis, M.; Vidakis, N. Three-Dimensional Printed Polylactic Acid (PLA) Surgical Retractors with Sonochemically Immobilized Silver Nanoparticles: The Next Generation of Low-Cost Antimicrobial Surgery Equipment. *Nanomaterials* **2020**, *10*, 985. [[CrossRef](#)]
26. Liebscher, M.; Gärtner, T.; Tzounis, L.; Mičušík, M.; Pötschke, P.; Stamm, M.; Heinrich, G.; Voit, B. Influence of the MWCNT surface functionalization on the thermoelectric properties of melt-mixed polycarbonate composites. *Compos. Sci. Technol.* **2014**, *101*, 133–138. [[CrossRef](#)]
27. Papageorgiou, D.G.; Tzounis, L.; Papageorgiou, G.Z.; Bikiaris, D.N.; Chrissafis, K.  $\beta$ -nucleated propylene-ethylene random copolymer filled with multi-walled carbon nanotubes: Mechanical, thermal and rheological properties. *Polymer* **2014**, *55*, 3758–3769. [[CrossRef](#)]
28. Terzopoulou, Z.; Patsiaoura, D.; Papageorgiou, D.G.; Pavlidou, E.; Chrissafis, K.; Tzounis, L.; Papageorgiou, G.Z.; Bikiaris, D.N. Effect of MWCNTs and their modification on crystallization and thermal degradation of poly(butylene naphthalate). *Thermochim. Acta* **2017**, *656*, 59–69. [[CrossRef](#)]
29. Tzounis, L.; Debnath, S.; Roj, S.; Fischer, D.; Mäder, E.; Das, A.; Stamm, M.; Heinrich, G. High performance natural rubber composites with a hierarchical reinforcement structure of carbon nanotube modified natural fibers. *Mater. Des.* **2014**, *58*, 1–11. [[CrossRef](#)]
30. Tzounis, L.; Kirsten, M.; Simon, F.; Mäder, E.; Stamm, M. The interphase microstructure and electrical properties of glass fibers covalently and non-covalently bonded with multiwall carbon nanotubes. *Carbon* **2014**, *73*, 310–324. [[CrossRef](#)]
31. Karalis, G.; Tzounis, L.; Lambrou, E.; Gergidis, L.N.; Paipetis, A.S. A carbon fiber thermoelectric generator integrated as a lamina within an 8-ply laminate epoxy composite: Efficient thermal energy harvesting by advanced structural materials. *Appl. Energy* **2019**, *253*, 113512. [[CrossRef](#)]
32. Tzounis, L.; Petousis, M.; Liebscher, M.; Grammatikos, S.; Vidakis, N. Three-Dimensional (3D) Conductive Network of CNT-Modified Short Jute Fiber-Reinforced Natural Rubber: Hierarchical CNT-Enabled Thermoelectric and Electrically Conductive Composite Interfaces. *Materials* **2020**, *13*, 2668. [[CrossRef](#)]
33. Li, Z.; Zabihi, O.; Wang, J.; Li, Q.; Wang, J.; Lei, W.; Naebe, M. Hydrophilic PAN based carbon nanofibres with improved graphitic structure and enhanced mechanical performance using ethylenediamine functionalized graphene. *RSC Adv.* **2017**, *7*, 2621–2628. [[CrossRef](#)]

34. Ferrari, A.C.; Basko, D.M. Raman spectroscopy as a versatile tool for studying the properties of graphene. *Nat. Nanotechnol.* **2013**, *8*, 235–246. [[CrossRef](#)] [[PubMed](#)]
35. Felisberto, M.; Tzounis, L.; Sacco, L.; Stamm, M.; Candal, R.; Rubiolo, G.H.; Goyanes, S. Carbon nanotubes grown on carbon fiber yarns by a low temperature CVD method: A significant enhancement of the interfacial adhesion between carbon fiber/epoxy matrix hierarchical composites. *Compos. Commun.* **2017**, *3*, 33–37. [[CrossRef](#)]
36. Bauhofer, W.; Kovacs, J.Z. A review and analysis of electrical percolation in carbon nanotube polymer composites. *Compos. Sci. Technol.* **2009**, *69*, 1486–1498. [[CrossRef](#)]
37. Coleman, J.N.; Khan, U.; Gun'ko, Y.K. Mechanical Reinforcement of Polymers Using Carbon Nanotubes. *Adv. Mater.* **2006**, *18*, 689–706. [[CrossRef](#)]
38. Wode, F.; Tzounis, L.; Kirsten, M.; Constantinou, M.; Georgopoulos, P.; Rangou, S.; Zafeiropoulos, N.E.; Avgeropoulos, A.; Stamm, M. Selective localization of multi-wall carbon nanotubes in homopolymer blends and a diblock copolymer. Rheological orientation studies of the final nanocomposites. *Polymer* **2012**, *53*, 4438–4447. [[CrossRef](#)]
39. Kapnopoulos, C.; Mekeridis, E.D.; Tzounis, L.; Polyzoidis, C.; Zachariadis, A.; Tsimikli, S.; Gravalidis, C.; Laskarakis, A.; Vouroutzis, N.; Logothetidis, S. Fully gravure printed organic photovoltaic modules: A straightforward process with a high potential for large scale production. *Sol. Energy Mater. Sol. Cells* **2016**, *144*, 724–731. [[CrossRef](#)]
40. Luo, J.; Cerretti, G.; Krause, B.; Zhang, L.; Otto, T.; Jenschke, W.; Ullrich, M.; Tremel, W.; Voit, B.; Pötschke, P. Polypropylene-based melt mixed composites with singlewalled carbon nanotubes for thermoelectric applications: Switching from p-type to n-type by the addition of polyethylene glycol. *Polymer* **2017**, *108*, 513–520. [[CrossRef](#)]
41. Moriarty, G.P.; De, S.; King, P.J.; Khan, U.; Via, M.; King, J.A.; Coleman, J.N.; Grunlan, J.C. Thermoelectric behavior of organic thin film nanocomposites. *J. Polym. Sci. Part B Polym. Phys.* **2013**, *51*, 119–123. [[CrossRef](#)]
42. Tzounis, L.; Gärtner, T.; Liebscher, M.; Pötschke, P.; Stamm, M.; Voit, B.; Heinrich, G. Influence of a cyclic butylene terephthalate oligomer on the processability and thermoelectric properties of polycarbonate/MWCNT nanocomposites. *Polymer* **2014**, *55*, 5381–5388. [[CrossRef](#)]
43. Tzounis, L.; Liebscher, M.; Tzounis, A.; Petinakis, E.; Paipetis, A.S.; Mäder, E.; Stamm, M. CNT-grafted glass fibers as a smart tool for epoxy cure monitoring, UV-sensing and thermal energy harvesting in model composites. *RSC Adv.* **2016**, *6*, 55514–55525. [[CrossRef](#)]



© 2020 by the authors. Licensee MDPI, Basel, Switzerland. This article is an open access article distributed under the terms and conditions of the Creative Commons Attribution (CC BY) license (<http://creativecommons.org/licenses/by/4.0/>).